Contrasting decay of historical building stone: Relationships between petro-physical feature and frontal polymerization treatment suitability on medieval building of north Sardinia (Italy).

Bulletin of Engineering Geology and the Environment

Contrasting decay of historical building stone: Relationships between petro-physical feature and frontal polymerization treatment suitability on medieval building of north Sardinia (Italy).

--Manuscript Draft--

Manuscript Number:	BOEG-D-17-00549R2
Full Title:	Contrasting decay of historical building stone: Relationships between petro-physical feature and frontal polymerization treatment suitability on medieval building of north Sardinia (Italy).
Article Type:	Original Article
Corresponding Author:	Stefano Cuccuru, Ph.D Universita degli Studi di Sassari Dipartimento di Scienze della Natura e del Territorio ITALY
Corresponding Author Secondary Information:	
Corresponding Author's Institution:	Universita degli Studi di Sassari Dipartimento di Scienze della Natura e del Territorio
Corresponding Author's Secondary Institution:	
First Author:	Stefano Cuccuru
First Author Secondary Information:	
Order of Authors:	Stefano Cuccuru
	Paola Mameli
	Alberto Mariani
	Paola Meloni
	Giacomo Oggiano
Order of Authors Secondary Information:	
Funding Information:	Regione Autonoma della Sardegna (P.O.R. Sardegna 2000-2006) — Not applicable
	Ministero per i beni culturali e l'ambiente — Not applicable
Abstract:	Textural, physical-mechanical, and mineralogical-chemical properties influence the degradation of building stone. These properties also control the efficacy of different preventative treatments to inhibit degradation. In this study, several historic buildings in northern Sardinia constructed with a wide variety of building stones were examined in order to contrast degradation effects with and without frontal polymerization. Different types of degradation were observed in carbonate and volcanic lithologies, which compromise their durability and toughness. Among the different lithotypes tested, four revealed a good response to the polymerization treatment. Textural and physical-mechanical evidences show that open porosity and capillary absorption control the suitability of this treatment. Laboratory tests on both untreated and treated specimens revealed a strong reduction of parameters directly related to decay (e.g., open porosity and water absorption), as well as an improvement on crush strength. Moreover, the polymerization treatment retains a residual porosity sufficient to enable the rock to equilibrate with the ambient environmental humidity.
Response to Reviewers:	The changes are illustrated in the rebuttal letter.

Ref.: BOEG-D-17-00549R1
Contrasting decay of historical building stone: Relationships between petro-physical feature and frontal polymerization treatment suitability on medieval building of north Sardinia (Italy).
Bulletin of Engineering Geology and the Environment

Dear Editor,

Here the revised manuscript with the new integrations required by the Reviewer #3.

In particular:

1) All red corrections have been removed and now the text shows only the final appearance;

2) “weak diagenesis” has been replaced by “low diagenesis”;

3) In the FIG 1, a small counter clockwise rotation (6°) in the general inset has been carried out.

Yours sincerely

Stefano Cuccuru

Contrasting decay of historical building stone: Relationships between petro-physical feature and frontal polymerization treatment suitability on medieval building of north Sardinia (Italy).

Cuccuru Stefano[1], Mameli Paola[1], Mariani Alberto[1], Meloni Paola[2], Oggiano Giacomo[1]

1 – Università di Sassari - Dipartimento di Chimica e Farmacia. Via Vienna 2, 07100 Sassari.

2 – Università di Cagliari – Dipartimento di Ingegneria Meccanica, Chimica e dei Materiali. Via Marengo 3, 09127 Cagliari.

Corresponding author: scuccuru@uniss.it - +39 079228633 - orcid.org/0000-0002-0175-3616

Abstract

Textural, physical–mechanical, and mineralogical–chemical properties influence the degradation of building stone. These properties also control the efficacy of different preventative treatments to inhibit degradation. In this study, several historic buildings in northern Sardinia constructed with a wide variety of building stones were examined in order to contrast degradation effects with and without frontal polymerization. Different types of degradation were observed in carbonate and volcanic lithologies, which compromise their durability and toughness. Among the different lithotypes tested, four revealed a good response to the polymerization treatment. Textural and physical–mechanical evidences show that open porosity and capillary absorption control the suitability of this treatment. Laboratory tests on both untreated and treated specimens revealed a strong reduction of parameters directly related to decay (e.g., open porosity and water absorption), as well as an improvement on crush strength. Moreover, the polymerization treatment retains a residual porosity sufficient to enable the rock to equilibrate with the ambient environmental humidity.

Key words:

Building conservation; building stones; rock mechanics; stone degradation; consolidation

1 INTRODUCTION

The Romanesque architecture in Sardinia (Italy) shows a wide range of characteristics. The buildings of this period reveal influences of Pisa, Lombardy, and Provence cultures related to the settlement of different religious orders, as well as craftsman of the Iberian Moresque culture. By the 13th century, the Franciscan order had introduced the Italian Gothic architectural and decorative style. Finally, in the 14th century after the Aragonese conquest, a cultural and artistic "catalanization" throughout Sardinia gave rise to several Catalan Gothic government and religious buildings.

The stone materials employed in medieval architecture reflect the local availability of building stone. The varied geology of Sardinia (Carmignani et al. 2016) provides a wide variety of building materials and dimension stones, including granites, sandstones, limestones, and in particular volcanic rocks. Such a variety of geological materials mean that building decay is highly variable, which has stimulated research on this topic.

The purpose of this study was to: (i) identify and characterize the materials used in some Romanesque and Gothic buildings of northern Sardinia; (ii) characterize the degradation of the building stones; (iii) identify historic quarries; (iv) test the effects of in situ frontal polymerization (FP) treatment (Vicini et al. 2005; Calia et al. 2013) taking into account the physical and textural natures of the different building stones.

2 MATERIALS AND METHODS

2.1 Buildings and their stones

This study focused on buildings located in a region corresponding to the medieval kingdom of Torres (northwest Sardinia) (Fig.1). In particular, we focused on the following five churches: Santa Maria Cathedral (Alghero) (Fig. 2a), Basilica of San Gavino (Porto Torres) (Fig. 2b), Nostra Signora del Regno (Ardara) (Fig. 2c), Basilica of Sant'Antioco di Bisarcio (Ozieri) (Fig. 2d), and Basilica of the Santissima Trinità di Saccargia (Codrongianos) (Fig. 2f). In addition, the 17th century building that hosts the administration of the University of Sassari (Fig. 2e) was examined, as this was constructed from the most common building stone in the region.

The survey of the different churches and their surroundings identified seven lithotypes of interest: sandstone (AR), yellow packstone (FER), white coarse-grained grainstone (PTW), green epiclastic sandstone (BISG), moderately welded ignimbrite (BIS), scoriaceous basalt (BAS), and white fine-grained packstone (SS).

The ancient extraction sites of the stones used for all the churches were successfully identified. Establishing the provenance of the building materials was of primary interest, not only for restoration and conservation purposes, but also to obtain sufficient quantities of samples to be tested. In a few cases, quarries were identified from historical documents, but in most cases geological surveys in the vicinities of the churches were necessary to identify the sources of the building materials. As such, a large amount of fresh material was available for laboratory analysis, including documenting textural, petrographic, and physical–mechanical properties, as well as FP treatment.

The Cathedral of Santa Maria is located in the historic center of Alghero (Fig. 2a). Its building began in the 16th century, but several later additions to the cathedral are known to have taken place, including the final addition of the neoclassical facade. The oldest structures and particularly the bell tower represent Gothic architecture. The building material is sandstone that crops out around Alghero and is locally called "Massacà" (AR). This lithotype crops out near Alghero, along the coast south of the town, and in the suburb of La Pietraia. Surveys identified several coastal quarries, where the eolian sandstone was quarried to be largely used in the town construction since its foundation under the Genoa republic.

The Basilica of San Gavino (Fig. 2b), located in Porto Torres, is the largest Romanesque church in Sardinia and stands on an ancient paleo-Christian zone of the Turris Libisonis Roman colony (Mastino et al. 1994). According to some historic documents (Coroneo 1993), the basilica already existed in the 11th century. The church was built by Pisan workers and shares its unusual foundations, characterized by opposing apses, with the coeval church of San Piero a Grado in Pisa. The size of the ashlars of the inner masonry match that of the carving cast found at Ferrinaggiu quarry, which is 2 km south of the basilica. The building stone provenance from this Roman and medieval extraction site was confirmed by petrographic study of micro-cores from the Basilica. The easy workability of the FER favored its indoor use for smooth ashlars, piers, and artifacts. Conversely, the weakness and high porosity of the marly calcarenite (FER) limited its exterior use, where a fossiliferous calcirudite (PTW) and fine-grained biosparite (SS) were preferred. The provenance of the PTW was identified in some still recognizable, but partially buried, Roman quarries in the western Porto Torres region. The SS is locally called "pietra columbrina" (Carta et al. 2005), and is widely found between Porto Torres and Sassari.

The Santa Maria del Regno Church (12th century) is located in Ardara village (Fig 2c). It was built in Pisan–Romanesque style with Lombard influences. Apart from rare pyroclastic rock ashlars in the facade, the church was mainly built with scoriaceous basalt (BAS). Due to the resistance of BAS to degradation, this church is a rare example of a church in the area that has not been heavily restored. This scoriaceous basalt comes from Pliocene–Quaternary lavas flows in this area (Mattioli et al. 2000). This lithotype has been widely used for building in Sardinia, due to its lightness with respect to other building materials.

The Basilica of Sant'Antioco di Bisarcio (Fig. 2d) was built between the 11th and 13th centuries, and is perhaps the most important basilica in Sardinia built with volcanic material. The church lies on a volcanic hill-top in the countryside near Ozieri. This Romanesque building has Pisan and Lombard stylistic influences. The building is E–W oriented, and has a central nave with an original wooden roof, separated by colonnades supporting arches along two lateral aisles with ribbed vaults. A moderately welded ignimbrite (BIS) was the dominant building material. This ignimbrite crops out widely around the church, and several small extraction sites were recognized. A fine-grained, greenish, epiclastic sandstone (BISG), cropping out north of the basilica, was used for dichromate inserts and decorations in two rows of ashlars on the church walls and more widely in the monastery wall.

The Basilica of Santissima Trinità di Saccargia (12th century) is perhaps the most famous and best example of Pisan–Romanesque basilicas in Sardinia (Fig. 2f). The church was entirely built with black basalt (BAS) and white limestone (equivalent to PTW and SS), which provide the contrasting coloration of a Tuscan Romanesque building. The plan of the church is a Latin cross

with a single nave ending in a transept with two chapels with ribbed vaults. Around the church, ruins of a monastery of the Camaldolese order are preserved, which was built with the same building stones (BAS, PTW, and SS).

2.2 Textural, mineralogical–petrographic, and physical–mechanical characterization

Mineralogical–petrographic and textural features of the building stones were studied in thin sections by optical microscopy. Alteration crusts and neo-formed minerals were examined by optical microscopy (ultra-thin sections) and an EVO LS10 scanning electron microscope with Oxford EDX and INCA-Xact microanalysis. The mineralogical compositions of all rock samples and patinas were determined by X-ray powder diffraction (XRPD) on a Bruker D2-Phaser diffractometer, equipped with a Cu X-ray tube, operating at 30 kV and 10 mA in the 6°–70° 2θ range. The XRD patterns were evaluated using the software EVA 4.1.1 (2015; Bruker DIFFRACplus Package) coupled with the database PDF-2 (ICDD).
To determine the physical–mechanical properties of the building stones we carried out the following set of tests according to UNI-EN standards (Tab. 1): dry density (UNI EN 9724/2), water absorption at atmospheric pressure (UNI EN 13755:2002), open porosity (UNI 9724/7), water absorption capillarity (UNI EN 1925:2000), and uniaxial compressive strength (UCS) (UNI EN 1926:2000).
Porosimetric measurements have been performed with a Hg Forced Intrusion (MIP) Micromeritics Autopore IV 9500 instrument, operating up to 2200 bars, equilibration time equal to 10 sec. Stone fragments of about 2 cm^3 were dried in stove at 60°C for 24 hours, then placed in a desiccator until cooling and finally weighed and introduced in a certified dilatometer.
In addition, an ultrasonic velocity test was performed with a CONTROLS 58-E0048 generator at 54 kHz. Measurements were made on all three pairs of sides of cubic samples (x, y, z).

All the listed tests were applied to the complete set of rock samples, and were repeated only on samples where FP proceeded successfully to assess the changes in the physical and mechanical properties.

The degradational features of the building stones were analyzed and classified in each building taking into account humidity, sun, and dominant wind exposure. In some cases, alteration crusts were sampled. The degradation was analyzed according to the NorMaL 1/88 Recommendation (1988) and following Fitzner and Heinrichs (2004).

2.3 Consolidation technique

Polymer impregnation improves the physical–mechanical properties of dimension stones and reduces the effects of weathering (Tsakalof et al. 2007). However, the high viscosity and average size of the polymeric macromolecules limit their efficiency, depending on the diameter and connectivity of pores within the material. In order to avoid this disadvantage, impregnation with monomers that undergo polymerization (the FP technique) has been tested (Vicini et al. 2005; Mariani et al. 2002). Prior to polymerization, all specimens (7x7x7 cm) were dried in a vacuum stove model Vuotomatic 50. After this, a monomer/initiator solution (1,6-hexanediol diacrylate–HDDA–2,2'-azo-bis/isobutirronitrile–AIBN; molar ratio 1:0.06) in an amount equal to ~30% of the weight of each rock was prepared. This solution was left to be absorbed into the building stone by capillarity. The polymerization reaction was then initiated, providing heat for the booster, by placing the specimens on a metal plate heated to 200°C for 90 s. The reaction is exothermic and self-propagating (Chechilo et al. 1972; Chekanov et al. 1997) and continues to spread through the specimens in a polymerization front, converting the absorbed monomer into a new polymeric compound.

3 RESULTS

3.1 Mineralogy and petrography

Sandstone (AR). The most common sandstone facies of this building stone is aeolian, although a coarser arenite deposited in a marine (shoreface) environment is also associated with this lithology. The rock has a clast-supported texture with sparry carbonate cement (Fig. 3a). The grains are well sorted and medium- to coarse-grained. In the marine facies, bioturbations are fairly common in the forms of *Skolithos* and *Diplocraterion* that result in relief in the degraded ashlars. Quartz, K-feldspar, plagioclase, heavy minerals, organogenic carbonate (red algae, bioclasts, and shell fragments) represent the detrital component. Occasionally, a fine fraction (1%) of reddish clays in the form of thin films partially coats the grains. The high degree of sorting and lack of matrix make this stone particularly porous (>30%, Table 2). Nevertheless, the calcite cement and abundance of siliciclasts means this material is quite resistant to degradation.

Yellowish packstone (FER). The degree of diagenesis of this rock is generally low. The lack of sedimentary structures observed in quarry cuts and texture of this rock indicate a medium–low energy sedimentary environment. According to Dunham (1962), this rock can be classified as a packstone. In thin section, fragments of algae (*Lithothamnium* and *Lithophyllum*), echinoids, benthic foraminifera, bryozoans, and rare Globigerinidae form the detrital component. The grains have a bimodal distribution, with maxima at 250 µm and 1 mm. A microcrystalline matrix (<10 µm) supports the grains. In addition to the (bio)-clastic components, subordinate angular quartz fragments (~50 µm), muscovite, biotite (chloritized), and rare microcline are present (Fig. 3b). Iron oxides are responsible for the yellowish staining of this rock. The occurrence of clay minerals and low levels of diagenesis make this lithotype easily workable compared with the other carbonate building stones.

White coarse-grained grainstone (PTW). This white stone is an algal macro-porous grainstone with cm-sized rhodoliths and bioclasts cemented by secondary, sparry calcite. Due to its macro-porous texture and the occurrence of abundant rhodoliths and sparry cement (Fig. 3c), this stone has a relatively low capillary absorption and high toughness (Table 2), which makes it suitable for use as basal ashlars and foundations.

Moderately welded ignimbrite (BIS). This is a brown–purple ignimbrite that is rhyodacitic in composition containing abundant xenoliths, which are predominantly andesites. In thin section, the vitroclastic texture has been partially obscured by devitrification processes. The vitrophyric matrix includes large anhedral phenocrysts of plagioclase (An_{30}) that are often fractured, and quartz. Pyroxene is generally altered to oxide and chloritic aggregates. Biotite occurs as small phenocrysts. Alkali feldspar is common as microcrystals. Xenoliths of metamorphic rocks are occasionally found in this rock. This ignimbrite is moderately welded and does not have a true eutaxitic texture; the shards in the matrix are not well oriented and slightly flattened pumice gives a weak planar anisotropy to this rock (Fig. 3d).

Green epiclastic sandstone (BISG). This rock comes from an epiclastic arenaceous deposit, which crops out north of the Basilica di Bisarcio. The sediments contain traces of *Thalassinoides* and have well developed stratification with centimeter to decimeter thick layers, which are easily splittable. The rock has experienced low diagenesis. Although graded bedding is common, the layers have a uniform grain size. This sandstone was derived from the erosion of silicic pyroclastic rocks and andesites. The grain size is sub-mm to mm in scale (Fig. 3e). In a Pettijohn diagram, the rock plots in the lithic–feldspathic greywacke field. The minerals present are plagioclase, quartz, biotite, altered pyroxene, and pumice fragments. The muddy matrix contains ash, along with greenish chlorite and rare calcite derived from the alteration of mafic minerals.

Scoriaceous basalt (BAS). The basalt used in the Santissima Trinità di Saccargia and Nostra Signora del Regno churches is always scoriaceous. The macro-porosity, due to its vesicular texture, can reach 40%. The interstitial lava is essentially glassy with a small percentage of microcrystals comprising plagioclase, pyroxene, and rare and weathered peridotite xenoliths. The overall stone color is black, with some reddish patches produced by local oxidizing conditions.

White fine-grained packstone (SS). This building stone is derived from the "calcari superiori" Formation (Mazzei and Oggiano 1990). Its distribution covers a wide area between Porto Torres and Sassari where it was largely quarried from, and locally is known as "pietra columbrina" (Carta et al. 2005). It is a packstone dominated by a microspar matrix, which contains slightly coarser dolomite crystals. The low levels of diagenesis and unimodal distribution of sub-mm-sized bioclasts give this rock a chalky texture (Fig. 3f). The low degree of diagenesis makes the stone easily workable for architectural and decorative purposes.

3.2 Physical and mechanical properties

Dry density: The BISG samples have the highest mean dry density value (Table 1), whereas the AR sample has the lowest dry density. This is consistent with the observed structures and textures as dry density is linked to textural features such as the occurrence of intergranular voids or vesicles.

Water absorption at atmospheric pressure: This test indicates the maximum water amount that the specimen absorbs by total immersion (saturation). The data shows large differences between the analyzed building stones (Table 1). The sample AR showed the highest water absorption, followed by samples FER, SS, and PTW. The lowest value characterizes the scoriaceous basalt (BAS), which has a closed vesicular porosity (see below) that hinders water infiltration.

Open porosity: The open porosity was calculated from the data obtained in the previous test as there is a direct correlation between open porosity and water absorption at atmospheric pressure. Hence, the values of this parameter mirror those of water absorption.

Mercury Intrusion Porosimetry: This technique is based on forced non-wetting liquid penetration into a porous material. The highest porosity values (>30%) were detected in sedimentary rocks. Conversely, scoriaceous basalt (BAS) due to the blind pores in a very compact glassy matrix, yielded the lowest MIP porosity

Water capillarity absorption: This test indicates the maximum quantity of water that the specimen absorbs by capillarity from one side immersed in deionized water. Taking into account the capillarity coefficient (C), the SS sample showed the highest value, followed by the AR, FER, and PTW samples (Table 1). The BAS sample absorbed the lowest water content.

Uniaxial compression strength: The uniaxial compression strength test showed that the volcanic building stones (BISG, BAS, and BIS) have high values, whereas the sedimentary samples were in general weaker (Table 1). In particular, the samples FER and AR had very low values due to their low levels of diagenesis. For this reason, these specimens disintegrated and collapsed.

Ultrasonic velocity: This test typically provides information about the presence of discontinuities in the rocks (e.g., fractures, pores, and cavities). The BAS sample provided the least resistance to the propagation of waves. In this case, the glassy structure allows the wave propagation into the specimens. Lower velocity values were recorded for the AR and FER samples (Table 1), due to the presence of intergranular voids that interfere with ultrasonic wave propagation.

3.3 Decay types

A combination of environmental factors along with intrinsic rock properties control the types of rock decay. Key factors are the exposure of walls, moisture in the foundations, and high evaporation rates that drive damp to rise through the walls. The most common types of degradation (alveolization, scaling, exfoliation, and disaggregation) are related to water action, including dissolution–recrystallization of soluble salts. Water in combination with other organic fluids also leads to efflorescences, patinas, stains, and crusts. In some cases, the pervasive heterogeneity of the rock allows degradation to progress in a way that causes selective weathering within the same ashlar. In northwestern Sardinia, marine aerosols (e.g., Zezza 1995) delivered by the dominant mistral wind are an important degradational factor on exposed surfaces.

Open porosity, water absorption, and capillarity absorption are related to rock texture, and exert a primary control on rock degradation (Pia et al. 2016; Carcangiu et al. 2015). Mineralogical and chemical compositions are also of relevance. For example, the durability of limestones like the SS is easily compromised by urban pollution. The calcareous SS, PTW, and FER building stones in the Basilica of San Gavino, Basilica of Santissima Trinità di Saccargia, and in some other buildings in Sassari share some of the same types of degradation as the volcanic building stones (e.g., alveolization and disaggregation–pulverization). In addition, these rocks are affected by karstic dissolution and experience recrystallization of gypsum in urban and coastal settings. Gypsum recrystallization is common in the SS ashlar buttresses of the old university palace in Sassari (Fig. 2e, Fig. 8b), which underwent treatment with an organic protective film. The desired

effect of these films is to improve the durability of the stone, but has caused abundant recrystallization of gypsum at the contact between the film and ashlar surface that underwent disintegration followed by detachment of the film (Fig. 8b). The degradation types observed in the SS samples are comparable with those identified in the PTW and FER samples. However, PTW shows a better resistance to decay due to its relatively low capillarity absorption with respect to SS and FER. Moreover, the inhomogeneous texture of PTW, characterized by large voids (up to 1 cm), hinders capillary rise of water. For this reason, the PTW building stone was extensively used in the basal ashlars of buildings, such as the Basilica of San Gavino, and where SS and FER are predominant in the internal walls. Some FER ashlars used for external masonry show deep alveolization or disintegration due to the dissolution of micritic matrix. Biological patinas mainly affect moisture-rich or shaded and damp surfaces. Some biological patinas have developed extensive vegetative colonization.

The volcanic and volcaniclastic building stones exhibit scaling and detachment, particularly on walls subjected to thermal extremes, such as those that are south-facing. Conversely, in north-facing walls microbiological colonization is common (e.g., Bisarcio). In general, alveolization prevails in less welded pyroclastic rocks and scaling in the most welded ignimbrites. Disintegration in the form of pulverization and alveolization particularly affects traceries and artifacts such as the stylophore lions and columns of Bisarcio. In this church, black crusts are also present inside niches and recesses where rain wash is not received. The crust is composed of whewellite ($CaC_2O_4.H_2O$) (Fig. 4, Fig. 6). The crusts are clearly related to a pigeon colony on the church, rather than transformation of an organic treatment as proposed by Alessandrini (1990) in similar situations. In fact, whewellite is associated with traces of nitrates and phosphates, as evidenced by SEM-EDS data (Fig. 4b).

The degradation of basalt building stone observed at Santa Maria del Regno and Saccargia is restricted to minor and diffuse alveolization in the scoriaceous facies. In contrast, the rare ignimbrite ashlars show exfoliation and alveolization.

Finally, only alveolization and disintegration affect the AR sandstone, which is principally due to the dissolution of the carbonate cement. In some ashlars with thin, cross-bedded stratification, selective decay has occurred, reflecting the differential diagenesis of each layer.

3.4 Effects of frontal polymerization

Not all the tested lithologies responded optimally to FP treatment. In fact, in some samples (BAS and BIS) polymerization started but was unable to spread more than 2–3 cm from the heat source through the specimens. This was due to incomplete imbibition as a result of inefficient capillary rise of the monomer within the specimens (Fig. 9), which particularly affected samples with low open porosity (e.g., BAS). However, excellent FP results were achieved in the sandstones and calcarenites (i.e., AR, FER, and SS), where the capillary rise of the monomer was effective. In these samples, FP successfully propagated throughout the specimens, although irregular FP behavior was recorded in the PTW sample.

After FP treatment, the samples were subjected to the same tests as the untreated samples (Table 2; Fig. 10; Fig. 11).

4 DISCUSSION AND CONCLUSIONS

The results of the FP treatment showed that only building stones with an open porosity above 20% and a capillarity absorption coefficient “C” (UNI EN 1925:2000) up to 30% are able to completely absorb the monomer/initiator solution, and allow complete propagation of the polymerization front (Fig. 12). The absence or partial propagation of polymerization reflects incomplete imbibition of the specimen (Fig. 9) and excess heat dissipation, with the latter preventing the threshold temperature necessary for the onset of FP being attained. As such, the thermal conductivity of the rocks exerts a control on the suitability of the FP method.

In detail, the dry density test identified an increase in weight per unit volume of the treated specimens, which reflects voids filled by the polymer. The average increase was ~15%, with a

maximum of 19% in the AR sample. There was a direct relationship between the density increase and open porosity. High water absorption values at atmospheric pressure are indicative of easy degradation, and hence a reduction in this parameter would be an ideal objective during treatment processes. The FP treatment produced a mean reduction of 82% in the building stones, with a minimum in the PTW sample. This low value for PTW reflects its heterogeneous textural domains, some of which prevented monomer penetration due to both its extreme compactness (rhodoliths and algae bioclasts) and the occurrence of large, and often unconnected, pores that hinder the capillary absorption of the monomer.

Open micro-porosity is the main parameter that allows water absorption and, on average, the open porosity decreased by 79% after FP treatment. In this case, the PTW sample had the least improvement because of incomplete polymerization. Figure 10 shows the dramatic drop in water absorption after FP treatment, which significantly improved the performance of the stones by reducing the coefficient "C" by a mean value of 91%.

MIP porosity - which is a dry technique - generally mirrored the behavior of open porosity inferred by water absorption. In any case the MIP drop after treatment was less evident due to the hydrophobic nature of the polymer. In the AR sandstone a reduction of the MIP porosity of about 41% was observed. The size pattern suggests that the polymer is able to permeate and fill small voids whereas, on voids of larger radius (≥ 6 μm), the main effect should result in a lining on the cavities walls by polymer formation; the new voids arrangement leaves a useful residual porosity which allows AR stone transpirating. A strong decrease in MIP porosity (about 46%) was observed for the SS specimens; the treatment produced evident obstruction of micrometric and submicrometric pores, but at the same time, it creates new open voids of larger size (Fig. 11a). On the FER, the treatment reduced the MIP of about 76%, without appearance of new voids population. The heterogeneous PTW limestone after PF treatment showed a remarkable reduction in MIP (about 50%) and a general modification of the voids distribution due to the filling of the micro-pores and appearance of a new pores population with larger size (Fig. 11b).Ultrasonic velocity is considered a diagnostic tool to verify the effects of building stone treatments (Ferreira Pinto and Delgado Rodrigues 2008). On average, the gain in velocity after FP treatment was 11.7%, with maximum values attained in the FER and AR samples. This enhancement reflects the pervasiveness of the polymer inside the rock voids.

The samples affected by complete propagation of the polymerization (AR, SS, and FER) exhibited a significant gain in crush strength, which on average was 268%. This behavior reflects the ability of the polymer to act as an adhesive that strongly enhances rock cohesion. In fact, the untreated AR, PTW, SS, and FER specimens broke by crumbling prior to treatment, and by fracturing after treatment.

In conclusion, the FP treatment proved useful and effective for a range of historic building stones from northern Sardinia. The open porosity, void size, and capillarity absorption coefficient are key controls on the suitability of this method. Overall, there was improved performance of the building stones and the treatment could counteract the different types of degradation detected in the considered buildings. In addition to the increase in crush strength and cohesion, the reduction in open porosity was significant, but the retention of a residual or new formed open porosity was optimal as this prevents entrapment of moisture in the masonry and allows it to easily equilibrate with the environmental humidity. The polymerization process resulted in filling of small pores, which are responsible of the strongest pressure of ice and salt crystallization, and was also responsible of larger voids.

Given the efficiency of the treatment, the next step in the project will cover the practical aspects of the FP application on the building facades with the design of an applicator able to inject the monomer/initiator solution inside the masonry and provide the heat able to trigger FP.

Acknowledgments:

This work was supported by the Regional Government of Sardinia (P.O.R. Sardegna 2000-2006 granted to Giacomo Oggiano) and by the Italian Ministry of cultural heritage (financial support funded to Paola Mameli). The authors are grateful to the referees for their valuable comments which helped to improve the manuscript.

References

Alessandrini G, Realini M (1990) Le pellicole ad ossalati: origine e significato nella conservazione. Arkos, 9/10, 19, 36.

Calia A., Colangiuli D., Lettieri M., Matera L. (2013) A deep knowledge of the behaviour of multi-component products for stone protection by an integrated analysis approach. Progress in Organic Coating, 76; 893-899

Carcangiu G, Casti M, Desogus G, Meloni P, Ricciu R (2015) Microclimatic monitoring of a semi-confined archaeological site affected by salt crystallisation. Journal of Cultural Heritage, 16, Issue 1: 13-118.

Carmignani L, Oggiano G, Funedda A, Conti P, Pasci S (2016) The geological map of Sardinia (Italy) at 1:250000 scale. Journal of Maps, 12: 826-835

Carta L, Calcaterra D, Cappelletti P, Langella A, de'Gennaro M (2005) The stone materials in the historical architecture of the ancient center of Sassari: distribution and state of conservation. Journal of Cultural Heritage 6: 277-286.

Chechilo NM, Khvilivitskii RJ, Enikolopyan NS (1972) On the Phenomenon of Polymerization Reaction Spreading. Dokl Akad Nauk SSSR, 204: 1180-1181.

Chekanov Y, Arrington D, Brust G, Pojman JA (1997) Frontal Curing of Epoxy Resin: Comparison of Mechanical and Thermal Properties to Batch Cured Materials. J Appl Polym Sci, 66: 1209-1216.

Coroneo R (1993) Architettura romanica dalla metà del Mille al primo '300. Collana "Storia dell'arte in Sardegna". Illisso, Nuoro.

Dunham RJ (1962) Classification of Carbonate Rocks According to Depositional Texture. In: Ham, W.E., Ed., Classification of Carbonate Rocks, AAPG, Tulsa, 108-121.

Ferreira Pinto AP, Delgado Rodrigues J (2008) Stone consolidation: the role of treatment procedures. Journal of cultural heritage, 9: 38-53

Fitzner B, Heinrichs K (2004) Photo atlas of weathering forms on stone monuments. http://www.stone.rwth-aachen.de

Mariani A, Fiori S, Pedemonte E, Pincin S, Princi E, Vicini S (2002) Consolidation Of Manufactured Objects Of Historical-Artistic Interest: Frontal Polymerization On Porous Substrates. ACS Polym. Prepr., 43: 869-870.

Mastino A, Vismara C (1994) Turris Libisonis. Collana "Sardegna archeologica. Guide e itinerari". Carlo Delfino, Sassari.

Mazzei R, Oggiano G (1990) Messa in evidenza di due cicli sedimentari nel Miocene dell'area di Florinas (Sardegna settentrionale). Atti Soc. Tosc. Sci. Nat. Mem. Ser. A, 97: 119-147.

Mattioli M, Guerrera F, Tramontana M, Raffaelli G, D'Atri M (2000) High-Mg Tertiary basalts in Southern Sardinia (Italy). Earth and Planetary Science Letters, 179:1-7.

NorMaL 1/88 (1988) Alterazioni macroscopiche dei materiali lapidei: lessico. ICR Roma – CNR Milano.

Pia G, Casnedi ML, Ricciu R, Besaluch LA, Cocco O, Murru A, Meloni P, Sanna UUM (2016) Thermal properties of porous stones in cultural heritage: Experimental findings and predictions using an intermingled fractal units model. Energy and Buildings, 118: 232-239.Tsakalof A, Manoudis P, Karapanagiotis I, Chryssoulakis I, Panayiotou C (2007) Assessment of synthetic polymeric coatings for the protection and preservation of stone monuments. J Cult Herit, 8: 69-72.

UNI 9724/7 (1992) Materiali lapidei—determinazione della massa volumica reale e della porosita` totale e accessibile

UNI EN 13755 (2002) Metodi di prova per pietre naturali—determinazione dell'assorbimento d'acqua a pressione atmosferica

UNI EN 1925 (2000) Metodi di prova per pietre naturali—determinazione del coefficiente di assorbimento d'acqua per capillarita

UNI EN 1926 (2000) Metodi di prova per pietre naturali—determinazione della resistenza a compressione

UNI 9724/2 (1990) Materiali lapidei—determinazione della massa volumica apparente e del coefficiente d'imbibizione

Vicini S, Mariani A, Princi E, Bidali S, Pincin S, Fiori S, Pedemonte E, Brunetti A (2005) Frontal polymerization of acrylic monomers for the consolidation of stone. Polymer Adv Tech, 16, 4, 293-298.

Zezza F, Macrì F (1995) Marine aerosol and stone decay. The science of the Total Environment 167 (1995) 123-143

Fig. 1 Study area showing the locations of buildings. (1) Santa Maria Cathedral, (2) Basilica of San Gavino, (3) Basilica of Sant'Antioco di Bisarcio, (4) Nostra Signora del Regno; (5) Basilica of the Santissima Trinità di Saccargia, and (6) University of Sassari

Fig. 2 a) Portal of Santa Maria Cathedral in Alghero, b) Basilica of San Gavino, c) Nostra Signora del Regno Church, d) Basilica of Sant'Antioco di Bisarcio, e) buttress of the old University Palace in Sassari, and f) Basilica of Santissima Trinità di Saccargia

Fig. 3 Thin section microphotos: a) AR (cross-polarized light), b) FER (cross-polarized light), c) PTW (cross-polarized light), d) BIS (plane-polarized light), e) BISG (plane-polarized light), f) SS (cross-polarized light).

Fig. 4 SEM images of BIS black patinas. a) Whewellite concretions and b) Phosphorous map

Fig. 5 SEM images of SS black crusts. a) Rosette-like microcrystalline gypsum and b) halite microcrystal

Fig. 6 XRD patterns of BIS patina and SS black crust showing peaks for neo-formed whewellite and gypsum, respectively

Fig. 7 XRD patterns of FER, PTW, and SS carbonate building stones

Fig. 8 a) Black patinas in BIS ashlars, b) Pulverization–disaggregation below gypsum-rich black crust in SS ashlars (Sassari), c) Selective degradation in AR sandstone, d) Alveolization in SS and PTW stones (S. Gavino), and e) Alveolization in scoriaceous basalt (Santa Maria del Regno)

Fig. 9 Different capillarity rise in the stones (incomplete in the volcanic rocks). From left: BAS, BISG, BIS, AR, FER, SS, PTW. Specimens side 7 cm

Fig. 10 Comparison of some physical–mechanical properties on untreated and FP treated samples

Fig. 11 Comparison of MIP of untreated and FP treated samples; a) AR, b) PTW, c) FERR, d) SS.

Fig. 12 Open porosity and capillarity absorption coefficient values of the different building stones. The dashed line represents the threshold below which FP treatment did not succeed due to a lack of front propagation

Table 1 Mean values of measured physical–mechanical properties

Table 2 Comparison of physical–mechanical properties between untreated and FP treated samples

Figure 1

Click here to download Figure FIG 1.tif

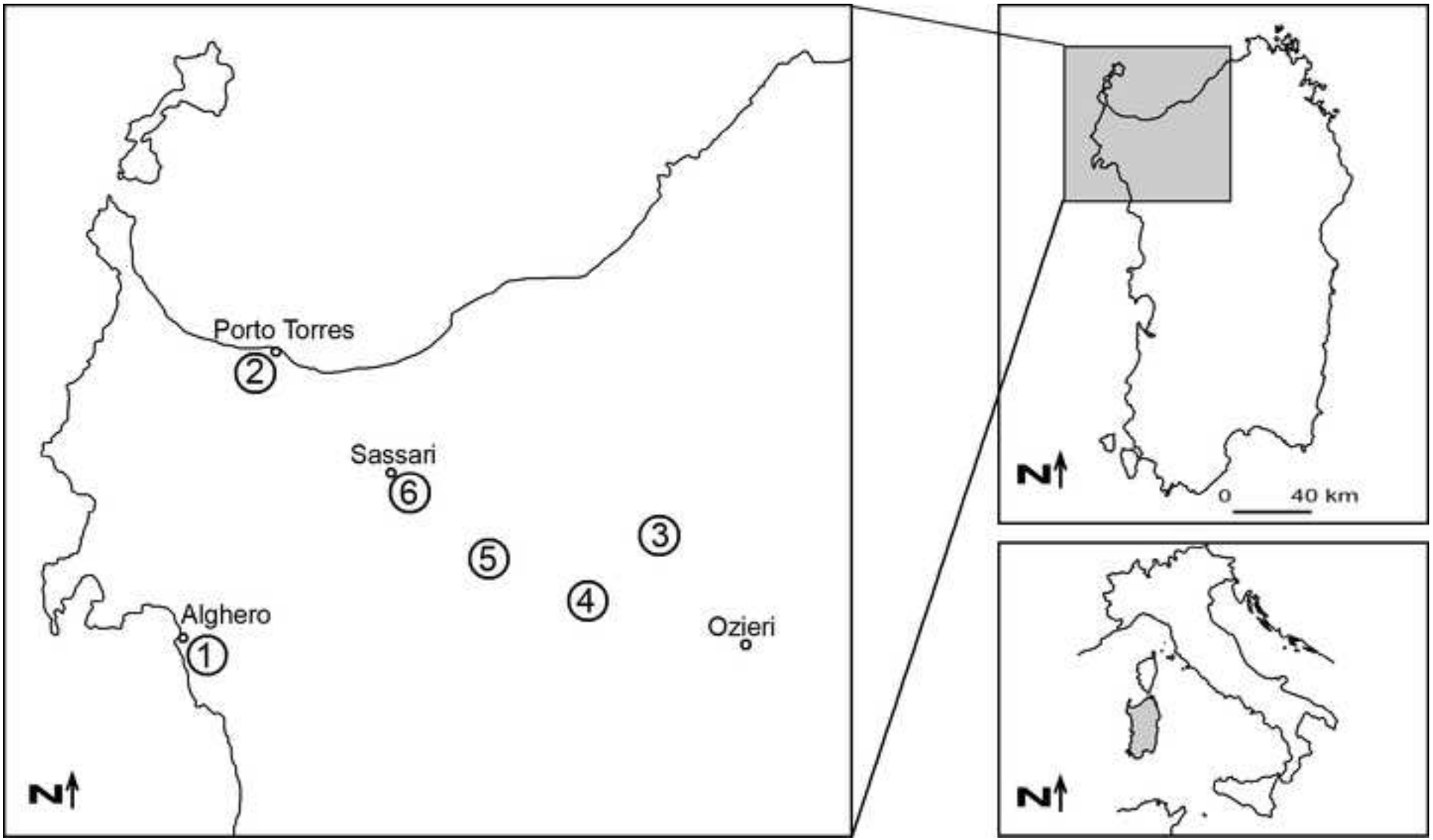

Figure 2

Click here to download Figure Fig 2.tif

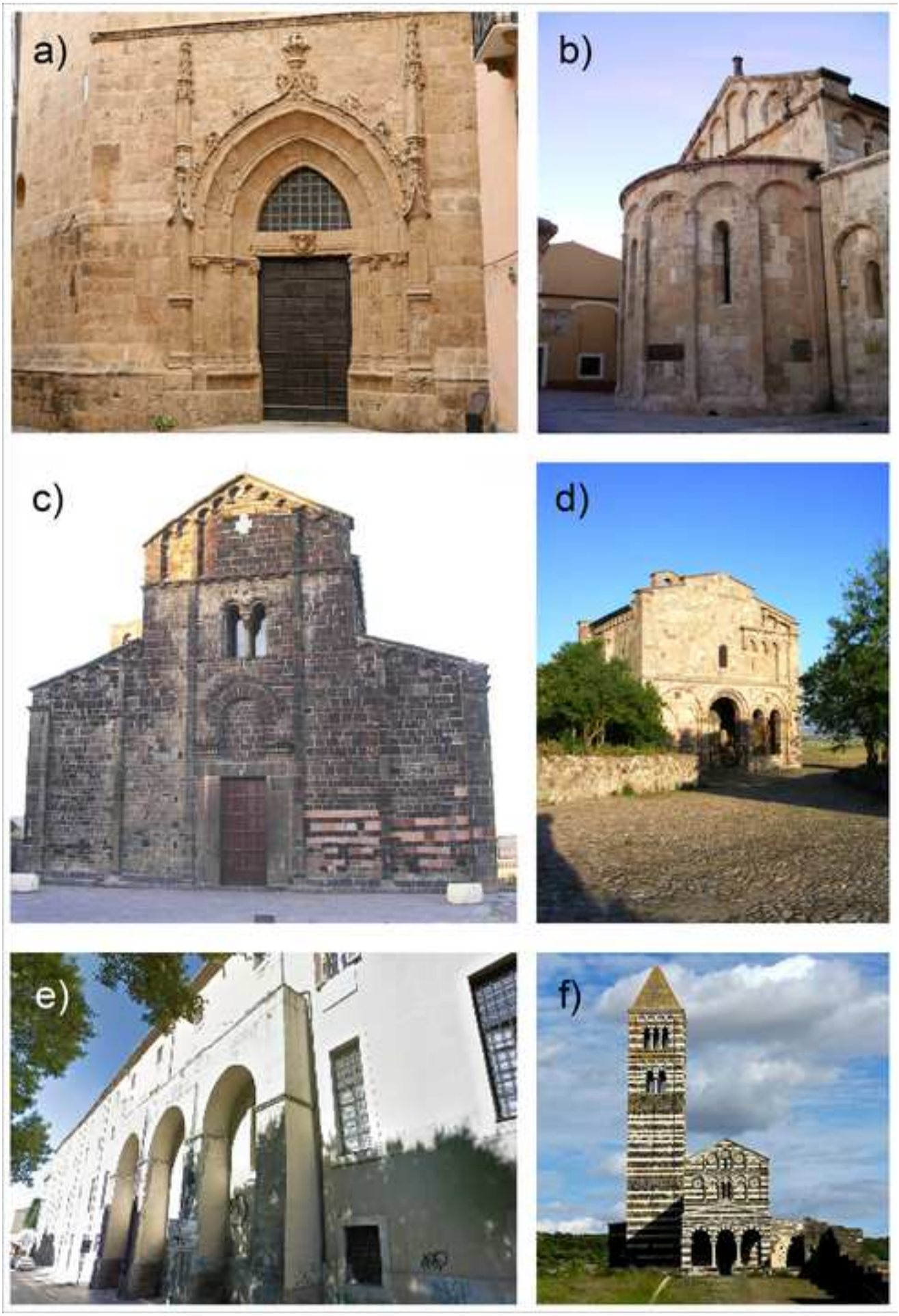

Figure 3

Click here to download Figure Fig 3.tif

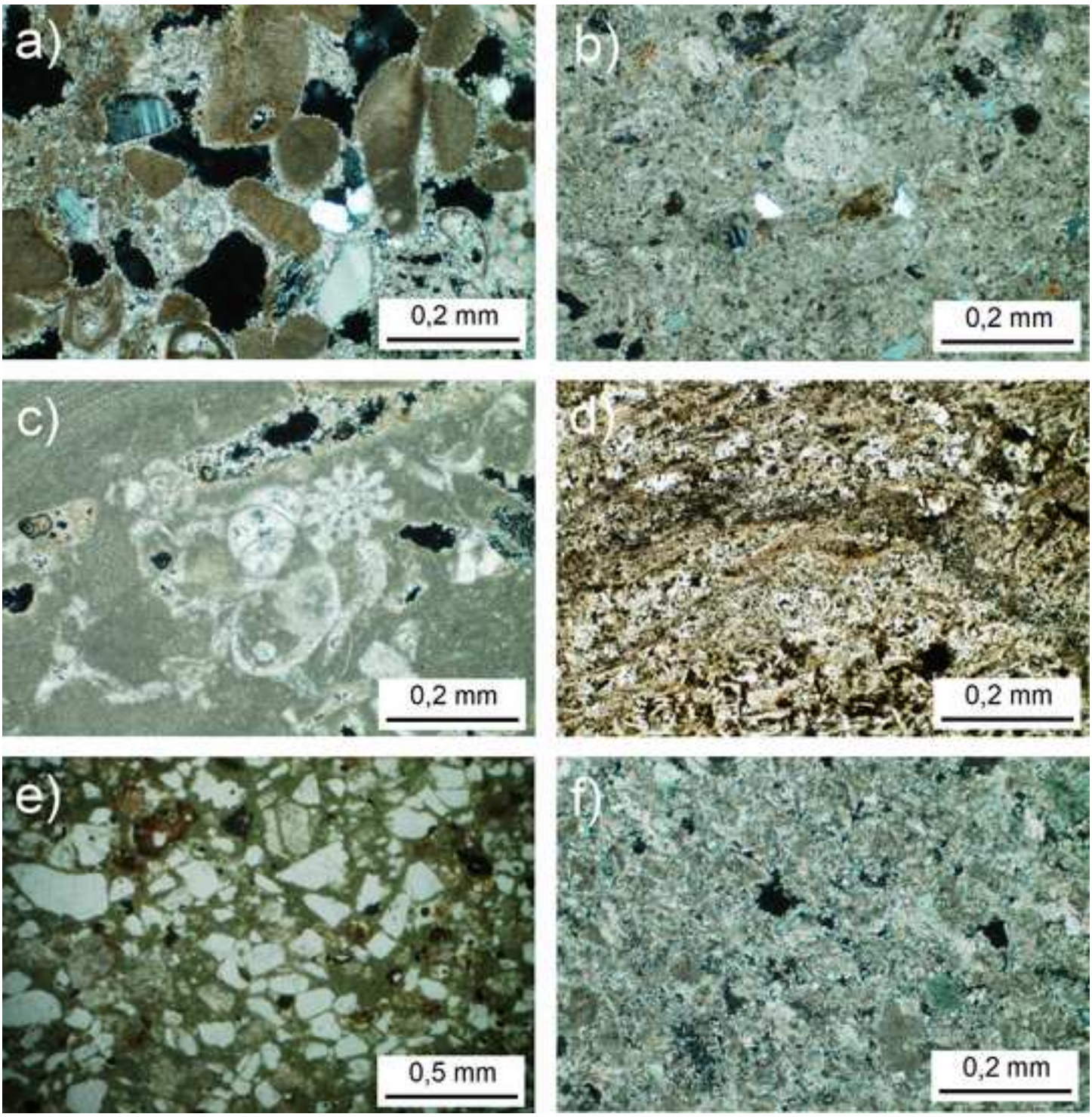

Figure 4

Click here to download Figure fig 4.tif

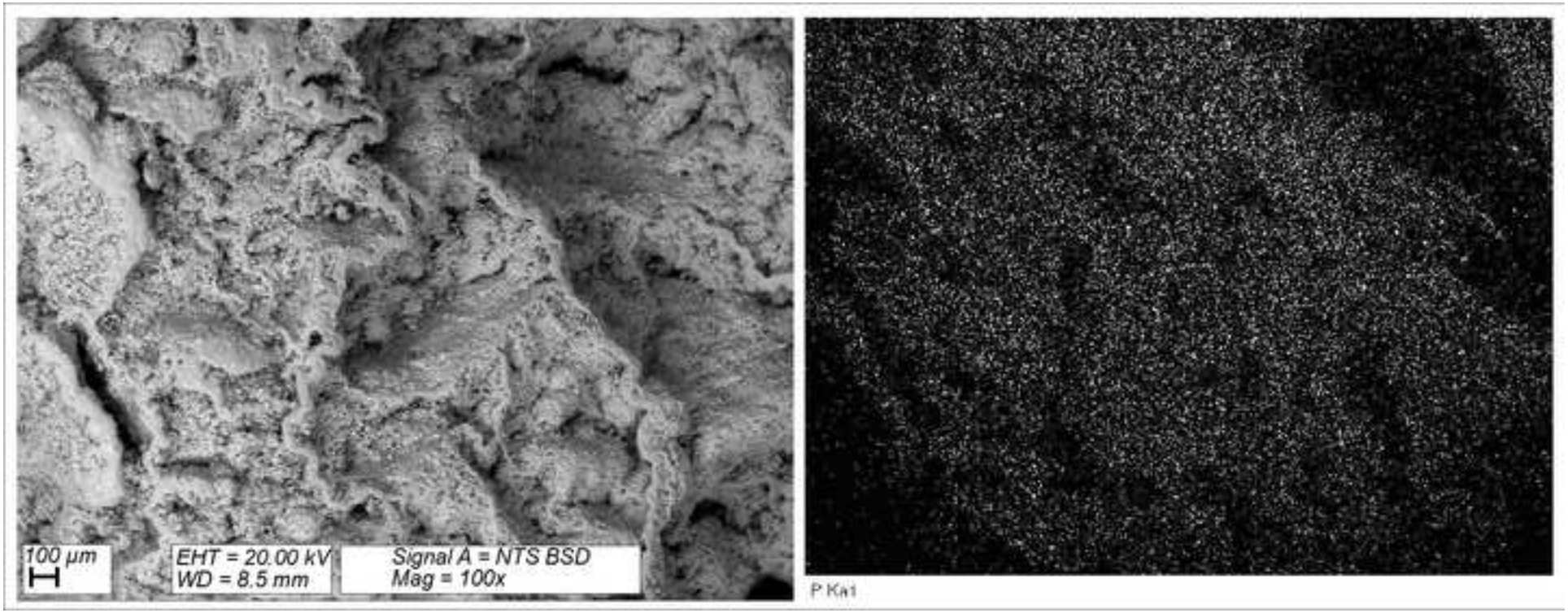

Figure 5

Click here to download Figure fig 5.tif

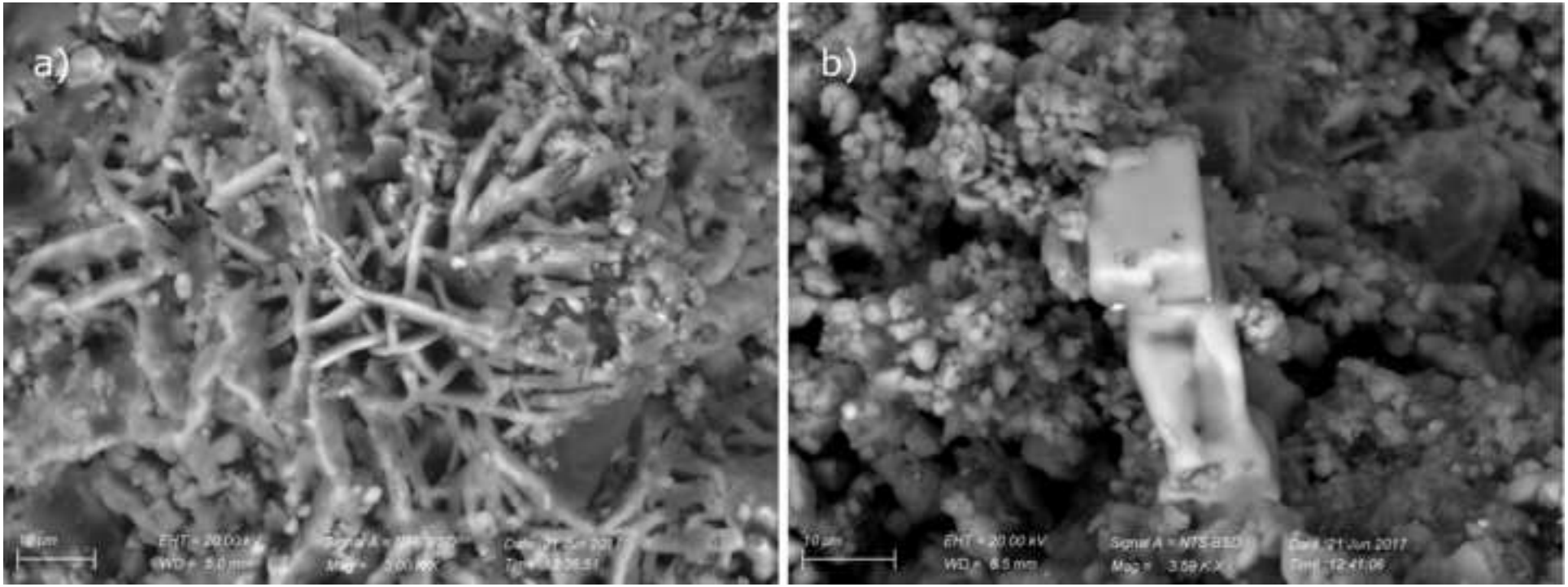

Figure 6

Click here to download Figure Fig 6.bmp

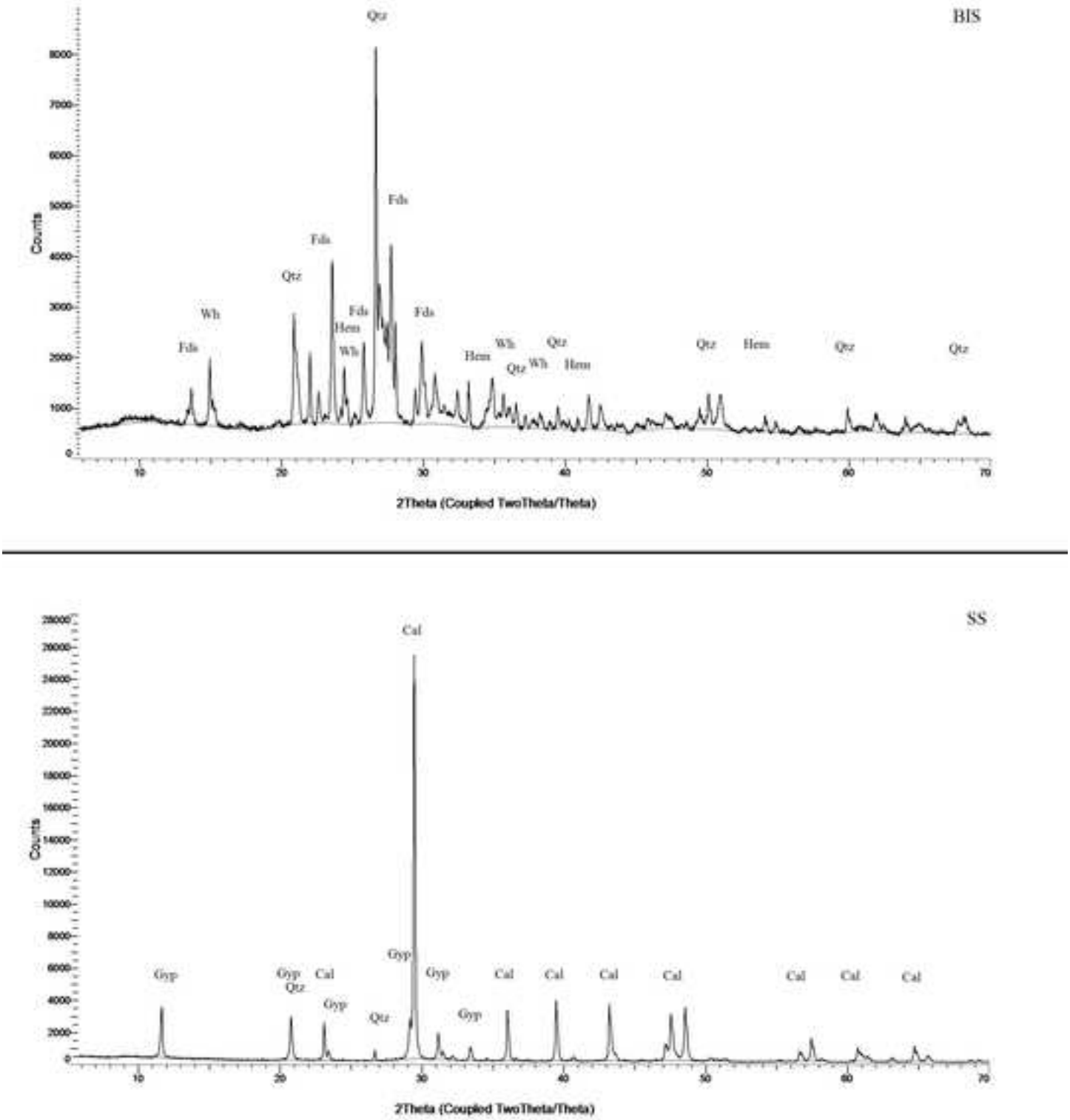

Figure 7

Click here to download Figure fig 7.jpg

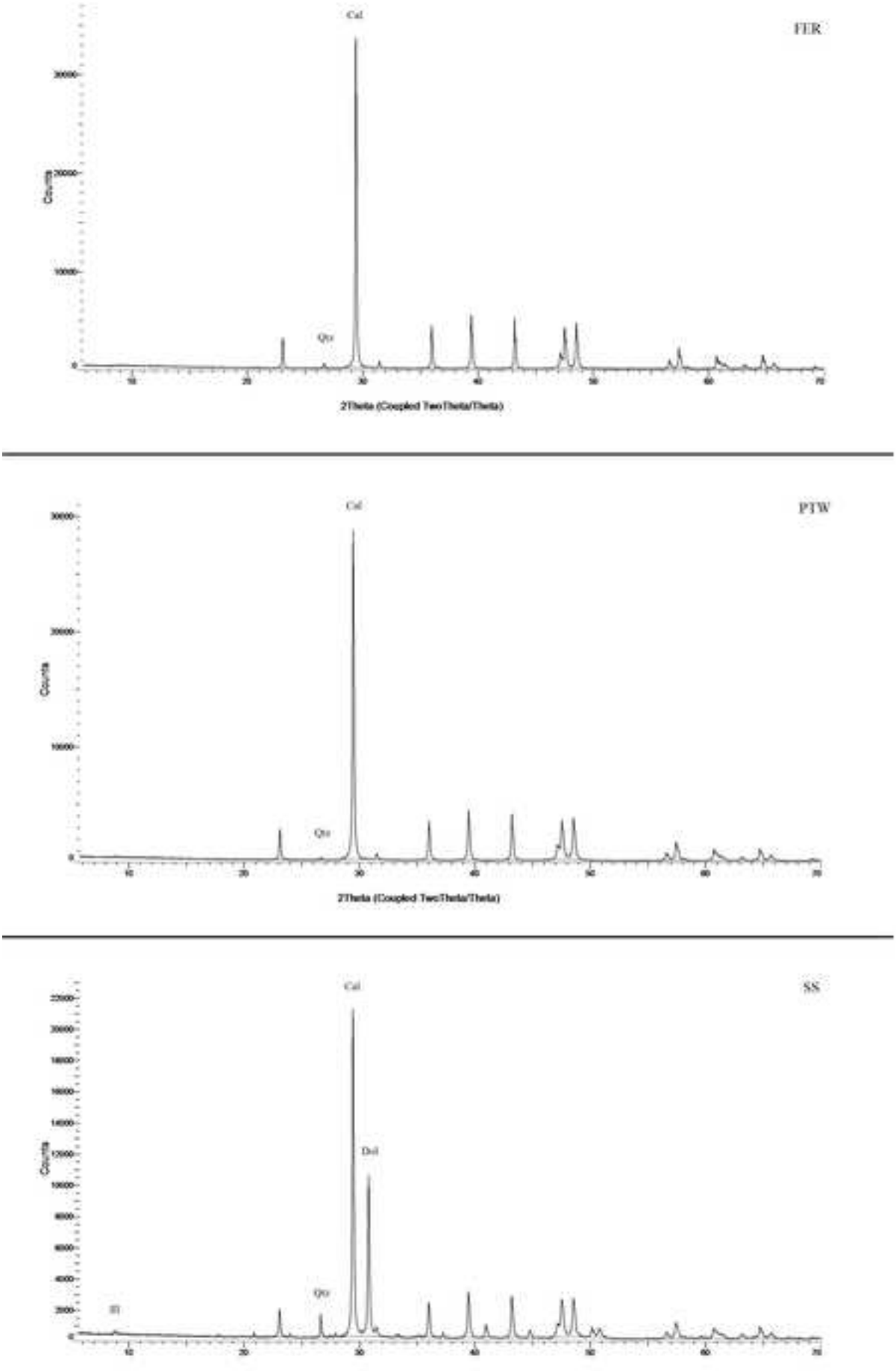

Figure 8

Click here to download Figure fig 8.tif

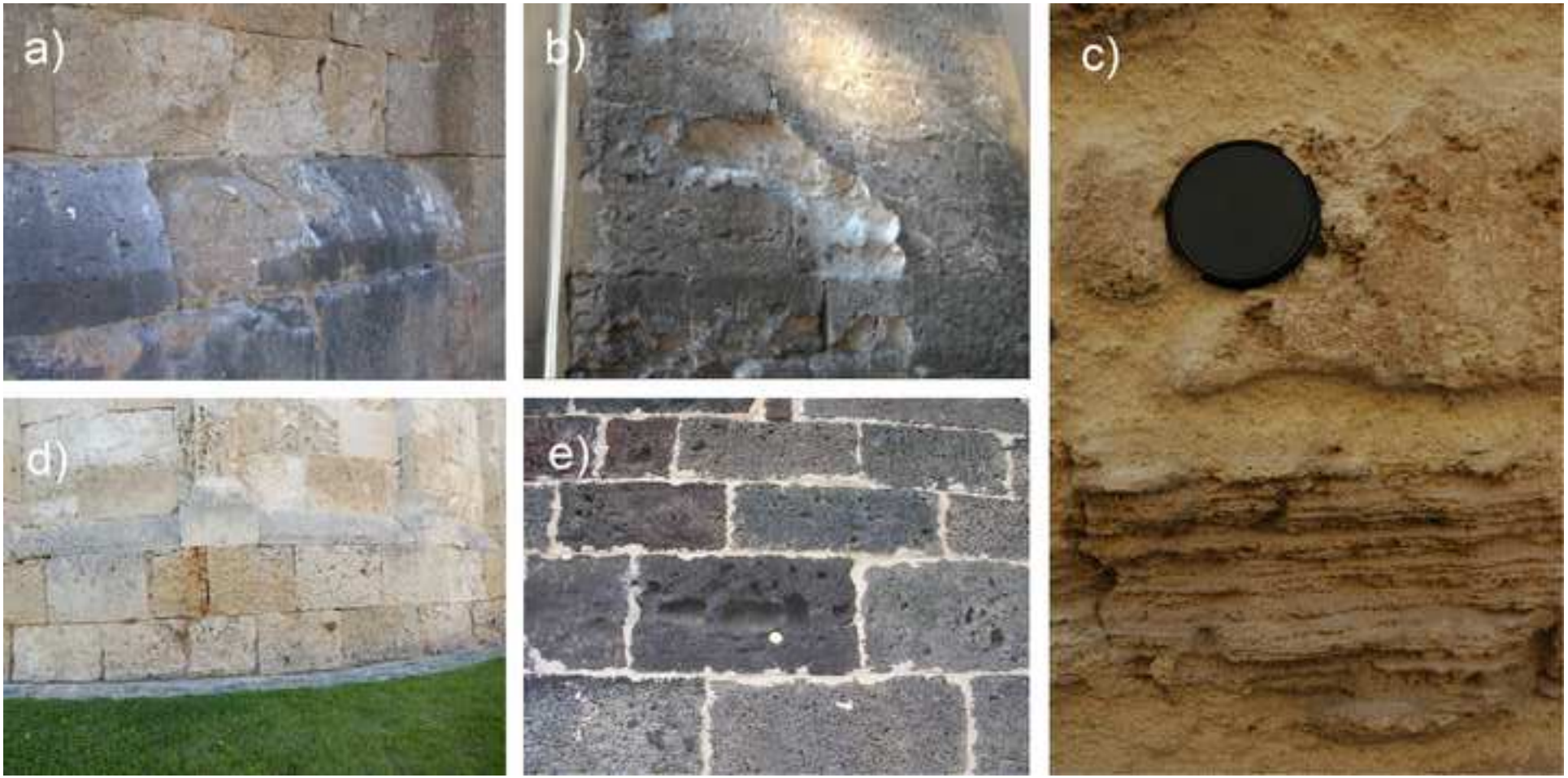

Figure 9

Click here to download Figure FIG 9.tif

Figure 10

Click here to download Figure fig 10.tif

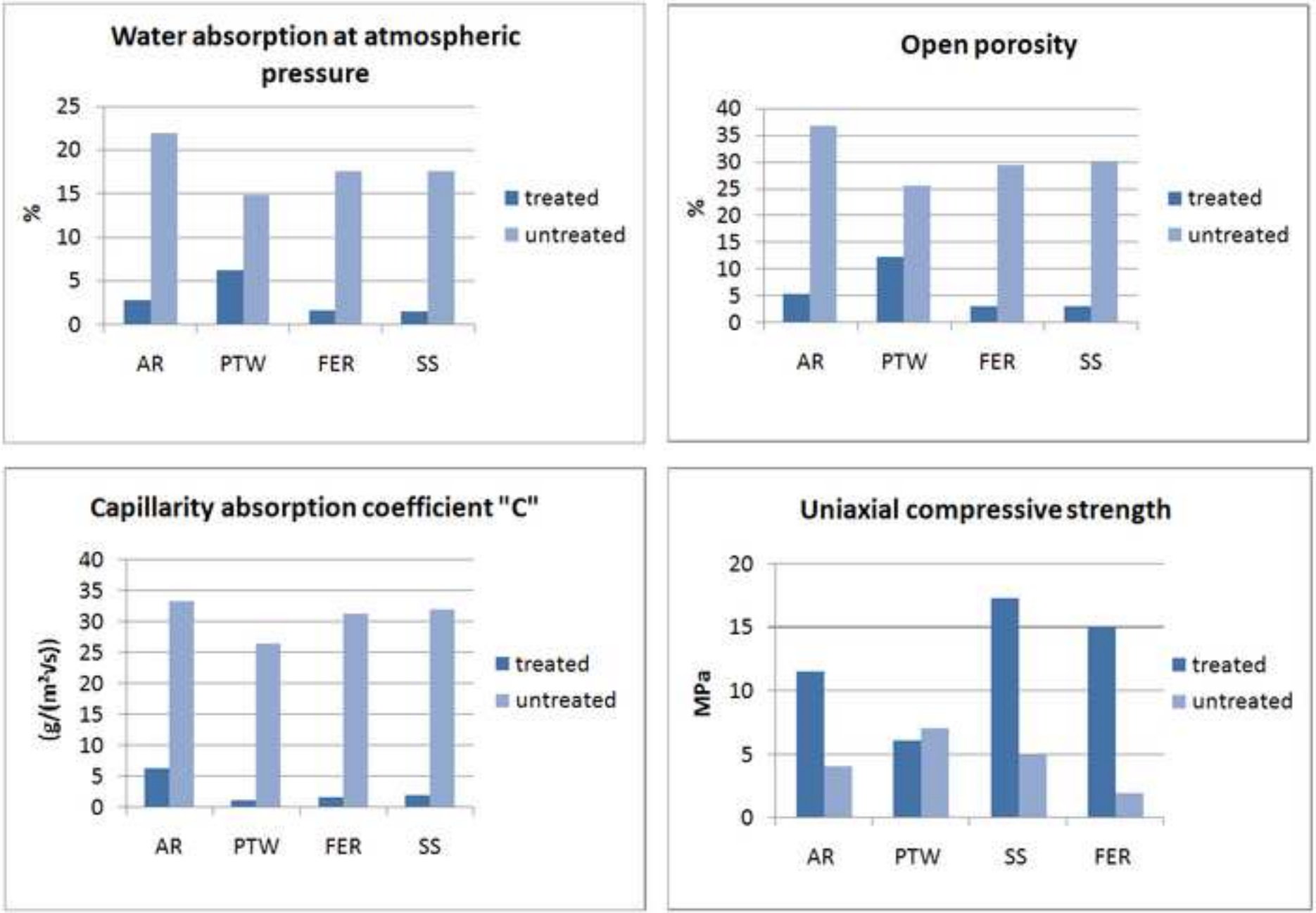

Figure 11

Click here to download Figure FIG 11.tif

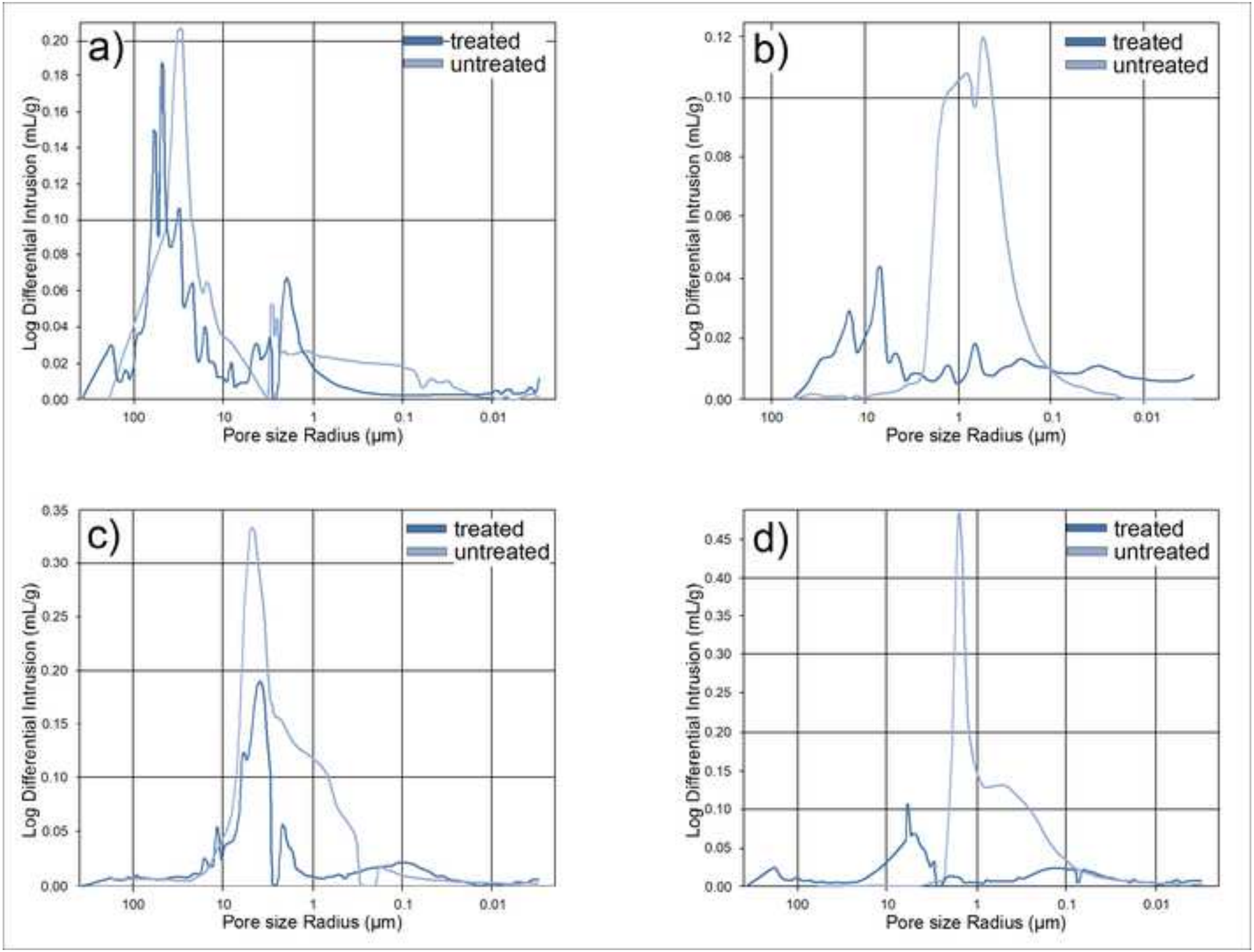

Figure 12

Click here to download Figure fig 12.tif

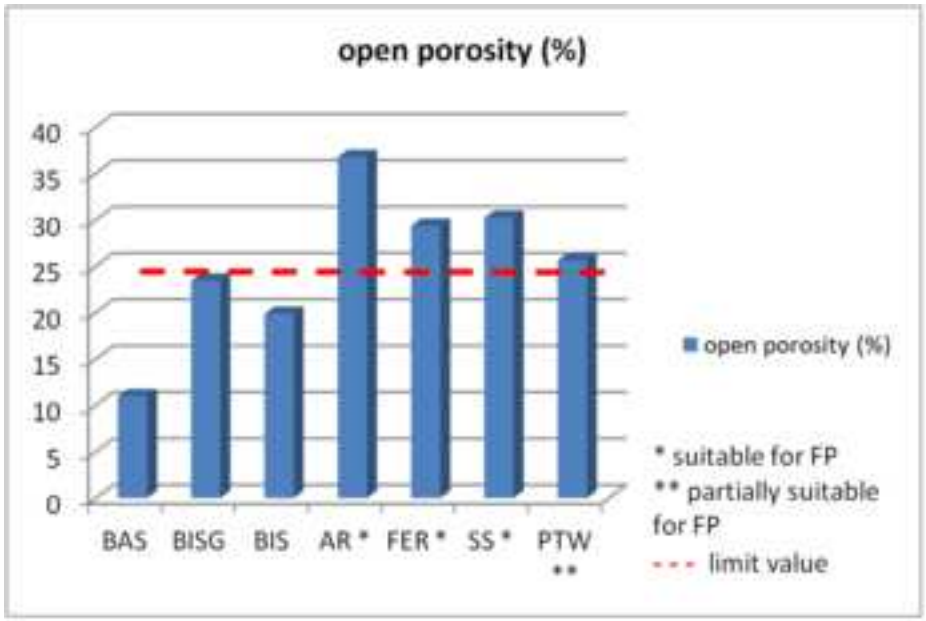

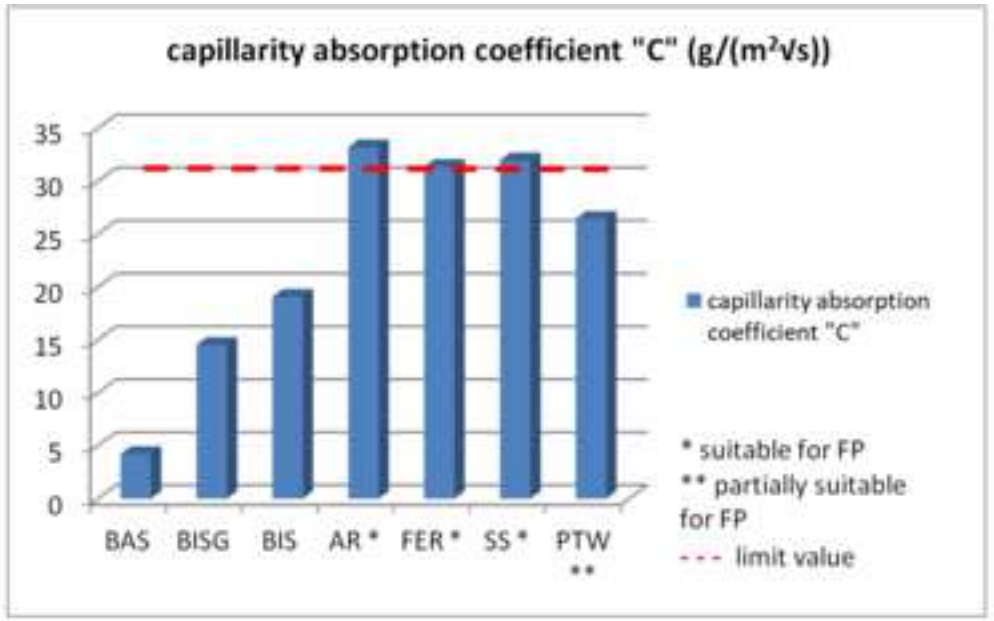

Table 1

Sample	Dry density	Water absorption at atmospheric pressure	Open porosity	Mercury intrusion porosimetry	Capillarity absorption coefficient “C”	Ultrasonic velocity	Uniaxial compressive strength
	mean values	mean values	mean values	mean values	mean values	mean values	mean values
	(g/cm^3)	(%)	(%)	(%)	($g/m^2 \sqrt{s}$)	(m/s)	(MPa)
BAS	1.99	5.28	10.96	13.97	4.22	3615	34.44
BISG	2.06	11.25	23.44	18.44	14.54	2736	38.09
BIS	1.79	11.26	19.83	19.76	19.09	2831	26.21
AR	1.66	21.96	36.76	30.40	33.38	2043	4.06
FER	1.67	17.57	29.33	36.84	31.36	2042	1.99
SS	1.72	17.6	30.21	32.53	31.98	2505	4.97
PTW	1.82	14.9	25.6	20.12	26.45	2742	7.07

Table 2

		Sample			
		AR	PTW	FER	SS
Dry density (g/cm^3)	Treated	1.97	1.99	1.91	1.99
	Untreated	1.66	1.82	1.67	1.72
	Variation %	19.06	9.41	14.41	16.04
Water absorption (%)	Treated	2.78	6.19	1.62	1.58
	Untreated	21.96	14.9	17.57	17.6
	Variation %	-87.35	-58.43	-90.8	-91.03
Open porosity (%)	Treated	5.48	12.34	3.09	3.14
	Untreated	36.76	25.6	29.33	30.21
	Variation %	-85.1	-51.81	-89.47	-89.6
Mercury intrusion porosimetry (%)	Treated	17.85	9.95	8.84	17.47
	Untreated	30.40	20.12	36.84	32.52
	Variation %	-41.3	-50.5	-76	-46.2
Capillarity absorption coefficient "C" (g/(m^2 vs))	Treated	6.31	1.17	1.67	1.96
	Untreated	33.38	26.45	31.36	31.98
	Variation %	-81.09	-95.56	-94.66	-93.86
Ultrasonic velocity (m/s)	Treated	2446	2925	2521	2431
	Untreated	2043	2742	2042	2505
	Variation %	19.72	6.69	23.46	-2.93
Uniaxial compressive strength (MPa)	Treated	11.55	6.12	15.08	17.35
	Untreated	4.06	7.07	1.99	4.97
	Variation %	184.63	-13.44	654.42	249.31